AIP Journal of Applied Physics

Predicted bond length variation in wurtzite and zinc-blende InGaN and AlGaN alloys

T. Mattila and Alex Zunger

Citation: Journal of Applied Physics **85**, 160 (1999); doi: 10.1063/1.369463
View online: http://dx.doi.org/10.1063/1.369463
View Table of Contents: http://scitation.aip.org/content/aip/journal/jap/85/1?ver=pdfcov
Published by the AIP Publishing

Predicted bond length variation in wurtzite and zinc-blende InGaN and AlGaN alloys

T. Mattila[a] and Alex Zunger[b]
National Renewable Energy Laboratory, Golden, Colorado 80401

(Received 20 July 1998; accepted for publication 5 October 1998)

Valence force field simulations utilizing large supercells are used to investigate the bond lengths in wurtzite and zinc-blende $In_xGa_{1-x}N$ and $Al_xGa_{1-x}N$ random alloys. We find that (i) while the first-neighbor cation–anion shell is split into two distinct values in both wurtzite and zinc-blende alloys ($R_{Ga-N_1} \neq R_{In-N_1}$), the second-neighbor cation–anion bonds are equal ($R_{Ga-N_2} = R_{In-N_2}$). (ii) The second-neighbor cation–anion bonds exhibit a crucial difference between wurtzite and zinc-blende binary structures: in wurtzite we find *two* bond distances which differ in length by 13% while in the zinc-blende structure there is only *one* bond length. This splitting is preserved in the alloy, and acts as a fingerprint, distinguishing the wurtzite from the zinc-blende structure. (iii) The small splitting of the first-neighbor cation–anion bonds in the wurtzite structure due to nonideal *c/a* ratio is preserved in the alloy, but is obscured by the bond length broadening. (iv) The cation–cation bond lengths exhibit three distinct values in the alloy (Ga–Ga, Ga–In, and In–In), while the anion–anion bonds are split into two values corresponding to N–Ga–N and N–In–N. (v) The cation–related splitting of the bonds and alloy broadening are considerably larger in InGaN alloy than in AlGaN alloy due to larger mismatch between the binary compounds. (vi) The calculated first-neighbor cation–anion and cation–cation bond lengths in $In_xGa_{1-x}N$ alloy are in good agreement with the available experimental data. The remaining bond lengths are provided as predictions. In particular, the predicted splitting for the second-neighbor cation–anion bonds in the wurtzite structure awaits experimental testing. © *1999 American Institute of Physics.* [S0021-8979(99)09601-2]

I. INTRODUCTION

The lattice constant *a(x)* of an isovalent $A_xB_{1-x}C$ semiconductor alloy, formed by constituents *AC* and *BC*, is known[1] to closely follow the composition-weighted average between the binary endpoints (Vegard's rule). In contrast, the nearest-neighbor bond lengths, $R_{A-C}(x)$ and $R_{B-C}(x)$ exhibit, in general, distinct values, resembling more their values in the individual binary constituents *AC* and *BC* rather than an average value corresponding to the virtual-crystal limit.[2–5] For alloys made of zinc-blende (ZB) constituents this has been explained theoretically using atomistic relaxation models.[3–8] For the alloys made of wurtzite (W) constituents, such as the III–V nitride alloys (InGaN, AlGaN, etc.), only very recent theoretical predictions[9] and experimental measurements[10] of the bond lengths have become available. The ground state of bulk-grown AlN, GaN, and InN is the W structure.[11–13] However, epitaxial stabilization[14] of ZB phase is possible.[11,12]

There are two significant, (and often overlooked) structural differences between the bond distances in ZB and W structures of binary compounds:

(i) The ZB structure has only one type of first-neighbor distance

$$R_{A-C}^{zb} = \frac{\sqrt{3}}{4} a_{zb} \quad \text{(four bonds)}, \tag{1}$$

where a_{zb} denotes the ZB lattice parameter, yet the W structure has *two* types of first-neighbor anion–cation bond distances (see Fig. 1):

$$\begin{aligned} R_{A-C_{1a}}^{w} &= u \frac{c}{a_w} \; a_w \quad \text{(one bond)} \\ R_{A-C_{1b}}^{w} &= \sqrt{\frac{1}{3} + \left(\frac{1}{2} - u\right)^2 (c/a_w)^2} \; a_w \quad \text{(three bonds)}, \end{aligned} \tag{2}$$

where u denotes the cell-internal structural parameter, a_w and c denote the lengths of the lattice vectors of the W structure (for description of the unit cell vectors see Ref. 13). In the case of an ideal tetragonal ratio $c/a_w = \sqrt{8/3} = 1.633$ and an ideal cell internal parameter $u = 3/8$ it follows from Eq. (2) that $R_{A-C_{1a}}^{w} = R_{A-C_{1b}}^{w}$. Using $c/a = 1.61$ and $u = 0.38$, resembling AlN or InN,[13] gives a difference $\leqslant 1\%$ between $R_{A-C_{1a}}^{w}$ and $R_{A-C_{1b}}^{w}$.

(ii) In the ZB structure we have only one type of second neighbor cation–anion bond distance

$$R_{A-C_2}^{zb} = \frac{\sqrt{11}}{4} \; a^{zb} \quad (12 \text{ bonds}). \tag{3}$$

On the other hand, the W structure has *three* types of second neighbor cation–anion distances connecting the cation *A* to anions C_{2a}, C_{2b}, and C_{2c} (see Fig. 1):

[a]Electronic mail: tmattila@nrel.gov
[b]Electronic mail: alex_zunger@nrel.gov

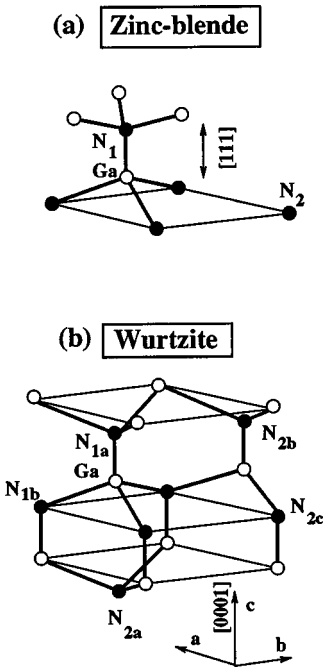

FIG. 1. The bond distances in (a) zinc-blende and (b) wurtzite structures. In the W structure there exist two first-neighbor bond lengths ($R^w_{A-C_{1a,b}}$), while in the ZB structure there is only one ($R^{zb}_{A-C_1}$). The second neighbor cation–anion distance in the W structure has three inequivalent values ($R^w_{A-C_{2a,b,c}}$), in contrast with the single bond length in the ZB structure ($R^{zb}_{A-C_2}$).

$$R^w_{A-C_{2a}} = (1-u)\frac{c}{a_w}\ a_w \quad \text{(one bond)}$$

$$R^w_{A-C_{2b}} = \sqrt{1+\left(\frac{uc}{a_w}\right)^2}\ a_w \quad \text{(six bonds)} \tag{4}$$

$$R^w_{A-C_{2c}} = \sqrt{\frac{4}{3}+\left(\frac{1}{2}-u\right)^2\left(\frac{c}{a_w}\right)^2}\ a_w \quad \text{(three bonds)}.$$

For ideal c/a_w and u we obtain

$$R^w_{A-C_{2a}} = \frac{5}{2\sqrt{6}}\ a_w = 1.0206\ a_w$$

$$R^w_{A-C_{2b}} = R^w_{A\text{-}C_{2c}} = \frac{\sqrt{11}}{2\sqrt{2}}\ a_w = 1.1726\ a_w\ . \tag{5}$$

Thus, even in the ideal W structure, $R^w_{A-C_{2a}}$ differs significantly (by 13%) from $R^w_{A-C_{2b}} = R^w_{A-C_{2c}}$. We note that this is much larger than the splitting in the first-neighbor shell [Eq. (2)].

In this article we explore the consequences of these differences between the ZB and W topologies in the *pure constituents* on the bond lengths in $In_xGa_{1-x}N$ and $Al_xGa_{1-x}N$ *random alloys*. The questions we ask in particular are whether the alloy environment acts to preserve or eliminate the distinction between (a) split bonds $R^w_{A-C_{1a}}$ vs $R^w_{A-C_{1b}}$ or between $R^w_{A-C_{2a}}$ vs $R^w_{A-C_{2b}}$ vs $R^w_{A-C_{2c}}$ of the *same* anion–cation *A–C* pair, and (b) the bonds *A–C* vs *B–C* of *different* cations *A* and *B*.

We find:

(i) *Split bonds of the same chemical species:* The effect of alloy broadening is larger than the difference between $R^w_{A-C_{1a}}$ and $R^w_{A-C_{1b}}$, but if one examines separately the nearest-neighbor bond parallel to the *c* axis ($R^w_{A-C_{1a}}$) and perpendicular to it ($R^w_{A-C_{1b}}$), one sees that they remain distinct in the alloy. Also, the splitting of the *second*-neighbor cation–anion distances $R^w_{A-C_{2a}}$ and $R^w_{A-C_{2b,c}}$ is preserved in the alloy. This splitting acts as a fingerprint distinguishing the W alloys from the ZB alloys.

(ii) *Bonds of different chemical species A–C vs B–C:* The splitting of the first-neighbor bond distances ($R_{A-C_1} \neq R_{B-C_1}$) is preserved, while the second-neighbor cation–anion distances R_{A-C_2} and R_{B-C_2} become nearly equal both in W and in ZB alloys (the splitting $R^w_{A-C_{2a}} \neq R^w_{A-C_{2b,c}}$ remains in W structure).

(iii) *Cation–cation and anion–anion bonds:* The first-neighbor cation–cation bonds R_{A-A}, R_{A-B}, and R_{B-B} show three distinct values. The first-neighbor anion–anion distance R_{C-C} is characterized by two distinct values corresponding to *C–A–C* and *C–B–C* configurations. These trends are explained based on the size mismatch of the cations *A* and *B*. The calculated cation–cation and anion–anion bonds have nearly identical values in W and ZB alloys.

(iv) *Bonds in* $Al_xGa_{1-x}N$ *vs* $In_xGa_{1-x}N$: The cation-related splittings *(A–C* vs *B–C)* are much larger for bonds in $In_xGa_{1-x}N$ than in $Al_xGa_{1-x}N$ due to larger size mismatch between the binary constituents GaN vs InN as compared with GaN vs AlN.

(v) Comparison of our results in $In_xGa_{1-x}N$ alloys with the recent experimental data[10] reveals good agreement for the first-neighbor cation–anion bonds and cation–cation bonds. The splitting between $R^w_{A-C_{2a}}$ and $R^w_{A-C_{2b,c}}$ in the W structure and the splitting of the anion–anion bonds are given as predictions to be tested experimentally.

II. METHODS

To find the relaxed atomic positions we have used the valence force field (VFF) method,[6,15,16] where the total strain energy is expressed as a function of atomic positions, $\{\mathbf{R}_i\}$, using a sum of bond stretching (V_2) and bond bending (V_3) terms:

$$\begin{aligned} E_{AE} &= \sum_{ij} V_2(\mathbf{R_i}-\mathbf{R_j}) + \sum_{ijk} V_3(\hat{\theta}_{ijk}) \\ &= \frac{1}{2}\sum_i \sum_j^{nn} \frac{3\alpha_{ij}}{8(d^0_{ij})^2}[(\mathbf{R_i}-\mathbf{R_j})^2-(d^0_{ij})^2]^2 \\ &\quad + \frac{1}{2}\sum_i \sum_{j,k>j}^{nn} \frac{3\beta_{i,jk}}{8d^0_{ij}d^0_{ij}}[(\mathbf{R_j}-\mathbf{R_i})\cdot(\mathbf{R_k}-\mathbf{R_i}) \\ &\quad - \cos\theta_0 d^0_{ij}d^0_{ij}]^2. \end{aligned} \tag{6}$$

Here, d^0_{ij} denotes the unstrained bond length between atoms *i* and *j*, and θ_0 is the unstrained bond angle, and $\cos\theta_0 = -1/3$. The bond stretching (α) and bond bending (β) force

TABLE I. The input ideal bond lengths d^0, the bond stretching (α), and bond bending (β) force constants used in the valence force field calculations.

Binary	d^0 (Å)	α (N/m)	β (N/m)
AlN	1.892	98.00	15.00
GaN	1.949	96.30	14.80
InN	2.156	79.20	7.10

TABLE II. The two VFF bonds lengths $d_{||}^0$ and $d_{\perp}^0$ used for nonideal *c/a* in the W structures [method (B)]. The values are derived based on the nonideal *c/a* ratio and cell internal parameter *u* for which we use the values calculated in Ref. 13.

Binary	*c/a*	*u*	$d_{||}^0$ (Å)	$d_{\perp}^0$ (Å)
GaN	1.633	0.378	1.968	1.947
InN	1.615	0.380	2.161	2.144

constants, derived from first-principles calculations,[17] are given in Table I. Also given in Table I are the input ideal bond lengths (d^0). In the alloys, we use the arithmetic mean for the bond bending (β) force constants for bond angle formed by atoms of mixed species (e.g., In–N–Ga). All the other parameters are kept at their binary values.

We describe the random alloy by large supercells with random occupation of the cation sites (thus, short-range order is neglected). In the W structure the supercell size was 1280 atoms ($8\times8\times5$ unit cells, the last dimension corresponding to the *c* axis), and in the ZB structure we used a simple cubic 512 atom supercell. Using different supercell sizes we have tested that our supercells give robust bond length distributions. The atomic relaxation was performed using the Fletcher-Reeves-Polak-Ribiere minimization algorithm.[18]

The lattice constants for the binary compounds are chosen to be consistent with the d^0 values. In the alloy systems the choice of the lattice constant *a(x)* requires further consideration. If the supercell volume (or lattice parameter) is given as an additional degree of freedom to be minimized during the relaxation, our VFF method results in a small downward bowing of the lattice parameter *a(x)* from the linear interpolation $\overline{a}(x)$ between the binary endpoints (Vegard's rule). In the zinc-blende $In_xGa_{1-x}N$ systems the calculated shift

$$\delta(x)=\frac{a(x)-\overline{a}(x)}{\overline{a}(x)}, \tag{7}$$

is -0.39% for $x=0.50$ and -0.30% for $x=0.25$ or 0.75. Even if we assume equal force constants at all atomic sites[8] [$\alpha(\mathrm{GaN})=\alpha(\mathrm{InN})$ and $\beta(\mathrm{GaN})=\beta(\mathrm{InN})$], the deviation $\delta(x)$ is -0.25% at $x=0.50$. Bulk-grown conventional III–V alloys exhibit experimentally[1,2] a range of deviations $\delta(x)$ from Vegard's rule. In $In_xGa_{1-x}As$ (Ref. 2) the deviation is very small, but in $In_xGa_{1-x}Sb$ (Ref. 1) it is large. In $In_xGa_{1-x}As$ VFF[6] gives $\delta(x=0.5)=-0.21\%$. Thus for this material VFF exaggerates the measured $\delta(x)$. We are not aware of any experimental data indicating how closely the lattice constant follows Vegard's law in InGaN and AlGaN alloys. Therefore we have decided to perform the calculations in two ways: (i) keeping the lattice constant (outer dimension of supercell) fixed to value predicted by Vegard's rule, and (ii) also relaxing the lattice constant during the minimization procedure. We present the detailed analysis of the bond lengths obtained using the two methods in Secs. III A for the ZB InGaN alloy (in AlGaN alloy the small lattice mismatch makes the deviation from Vegard's law much smaller and is therefore not considered). The results show that the difference in all of the investigated bond lengths obtained by methods (i) and (ii) simply correspond to scaling of the calculated bond lengths by the change $\delta(x)$ of Eq. (7).

In order to investigate the effect of deviations from perfect tetrahedral geometry in the W structure, we have separated the ideal VFF bond length into two values labeled $d_{||}^0$ (corresponding to $R_{A-C_{1a}}^w$, parallel to the *c* axis) and $d_{\perp}^0$ ($R_{A-C_{1b}}^w$, perpendicular to the *c* axis). We then proceed with two methods:

(A) We assume an ideal *c/a* axial ratio (equal to $\sqrt{8/3}$) and an ideal cell internal parameter *u* (equal to 3/8), and thus $d_{||}^0=d_{\perp}^0$. This corresponds to conserving perfect tetrahedral geometry in the W structure.

(B) We assume a nonideal *c/a* ratio and *u* based on the available experimental and first-principles values,[13] and adjust $d_{||}^0$ and $d_{\perp}^0$ accordingly for the binaries. The resulting values for $d_{||}^0$ and $d_{\perp}^0$ in InN and GaN are shown in Table II. We note that the weighted average (one $d_{||}^0$ bond, three $d_{\perp}^0$ bonds) yields 1.952 (2.148) Å for the Ga–N (In–N) bond with method (B), which is slightly larger (smaller) than 1.949 (2.156) Å for the ideal *c/a* [method (A)]. Based on this, for the Ga–N bond we expect a small average expansion when moving from the ideal to nonideal *c/a* structure, while the In–N bond is expected to contract with a slightly larger magnitude than the Ga–N expands. The remaining VFF parameters are kept at the values shown in Table I. In the alloy systems we assume a composition weighted *c/a* ratio between the two binary values.

In Sec. III B we use both methods (A) and (B) to study in detail $R_{A-C_{1a}}^w$ and $R_{A-C_{1b}}^w$ bonds in the W $In_{0.50}Ga_{0.50}N$ alloy. The results indicate only marginal difference between the bond lengths given by two methods in the alloy environment. Therefore, in the remaining calculations involving longer bonds we proceed only with approach (A) assuming perfect tetrahedral geometry for the W structure.

III. BOND LENGTHS IN $In_xGa_{1-x}N$ ALLOYS

A. Fixed vs relaxed lattice constant

As described in Sec. II, the applied VFF method predicts slightly deviating lattice parameter values from Vegard's law (linear interpolation between binary endpoints) for the $In_xGa_{1-x}N$ alloy systems. To quantify how the change in the lattice parameter is propagated into bond lengths, Table III shows bond lengths calculated using three methods: (V) keeping the lattice parameter fixed to the value given by Vegard's law and relaxing only the atomic positions, (R) relaxing both the atomic positions and lattice parameter, and (S) scaling the values obtained with method V by the con-

TABLE III. Comparison of the relaxed bond lengths (in angstroms) in zinc-blende $In_xGa_{1-x}N$ alloy as calculated using three methods: (V) Relaxing atomic positions while keeping the lattice parameter fixed to the value given by Vegard's rule, (R) relaxing the lattice parameter in addition to atomic positions, and (S) like V but scaling the bond lengths by the change $\delta(x)$ in lattice parameter. $\delta(x)$ equals -0.39% for $x=0.50$, and -0.30% for $x=0.25$ or 0.75.

x	Method	$R_{\text{Ga-N}_1}$	$R_{\text{In-N}_1}$	$R_{\text{Ga-N}_2}$	$R_{\text{In-N}_2}$	$R_{\text{Ga-Ga}}$	$R_{\text{Ga-In}}$	$R_{\text{In-In}}$	$R_{\text{N-N}_a}$	$R_{\text{N-N}_b}$
0.25	V	1.9633	2.1255	3.8311	3.8385	3.2428	3.2964	3.3208	3.2039	3.4707
0.25	R	1.9574	2.1195	3.8198	3.8271	3.2331	3.2869	3.3108	3.1943	3.4609
0.25	S	1.9574	2.1191	3.8196	3.8270	3.2330	3.2865	3.3109	3.1943	3.4603
0.50	V	1.9730	2.1408	3.9259	3.9398	3.2965	3.3549	3.4050	3.2176	3.4955
0.50	R	1.9651	2.1327	3.9106	3.9244	3.2832	3.3419	3.3918	3.2046	3.4823
0.50	S	1.9653	2.1324	3.9106	3.9245	3.2836	3.3418	3.3918	3.2050	3.4818
0.75	V	1.9783	2.1511	4.0198	4.0354	3.3371	3.4124	3.4650	3.2275	3.5108
0.75	R	1.9721	2.1449	4.0080	4.0235	3.3266	3.4023	3.4549	3.2175	3.5006
0.75	S	1.9723	2.1446	4.0077	4.0233	3.3271	3.4022	3.4546	3.2178	3.5003

traction in lattice parameter $\delta(x)$ [Eq. (7)]. We see that the bond lengths obtained using method S reproduce very accurately the bonds with method R (the differences occur in the fourth decimal). In other words, the ratio between the bond lengths in calculations V and R is the same as the ratio between the lattice parameters in the two calculations. This indicates that allowing the lattice constant to relax does not lead to significant structural changes in the system but the change is directly propagated into bond lengths and the relative lengths of different bonds remain the same. Therefore, in the following we will use Vegard's rule to extract bond length values. To account for deviation from Vegard's rule, all bond lengths in Table IV can be multiplied by $\delta(x)$ of Eq. (7).

B. First-neighbor cation–anion bonds: $R^w_{A-C_{1a}}$ vs $R^w_{A-C_{1b}}$

Figure 2 compares the first-neighbor cation–anion bonds in the W $In_{0.5}Ga_{0.5}N$ alloy as calculated using the two VFF models described in Sec. II. Figure 2(a) corresponds to the VFF calculation assuming ideal *c/a* ratio [method (A)], while Fig. 2(b) shows the result for nonideal *c/a* [method (B)]. In Fig. 2(b) we decompose the nearest-neighbor bond length distribution ($R^w_{A-C_1}$) into bonds parallel to the W *c* axis ($R^w_{A-C_{1a}}$) and perpendicular to it ($R^w_{A-C_{1b}}$). The decomposed bond lengths indicate that for both cation species the $R^w_{A-C_{1a}}$ bond is slightly longer than $R^w_{A-C_{1b}}$. However, this distinction is not visible in the combined $R^w_{A-C_1}$ bond distribution (the uppermost of the three histograms for each cation species in Fig. 2). Thus, we conclude that the difference between $R^w_{A-C_{1a}}$ and $R^w_{A-C_{1b}}$ bonds is preserved in the alloy environment, but simultaneously becomes obscured due to the statistical bond length broadening.

We further note that the R_{A-C_1} peak positions do not coincide between Figs. 2(a) and 2(b). The calculated average peak positions for the ideal (nonideal) *c/a* ratio are $R_{\text{Ga-N}_1}=1.973$ (1.974) Å and $R_{\text{In-N}_1}=2.141$ (2.132)Å, respectively. These differences can be understood as a consequence of the ideal (VFF) bond lengths assumed in methods (A) and

TABLE IV. Calculated values of the histogram (Fig. 3) average relaxed bond lengths (in angstroms) in $In_xGa_{1-x}N$ alloy for various compositions. The experimental values are from Ref. 10. For W structure an ideal *c/a* ratio is assumed in the calculations.

x	Structure	$R_{\text{Ga-N}_1}$	$R_{\text{In-N}_1}$	$R_{\text{Ga-N}_{2a}}$	$R_{\text{Ga-N}_{2b}}$	$R_{\text{In-N}_{2a}}$	$R_{\text{In-N}_{2b}}$	$R_{\text{Ga-Ga}}$	$R_{\text{Ga-In}}$	$R_{\text{In-In}}$	$R_{\text{N-N}_a}$	$R_{\text{N-N}_b}$
0.0	W	1.949		3.248	3.732			3.183			3.183	
0.0	ZB	1.949		3.732	3.732			3.183			2.183	
0.0	Exp.	1.94						3.19				
0.25	W	1.963	2.126	3.339	3.831	3.322	3.839	3.243	3.297	3.317	3.204	3.471
0.25	ZB	1.963	2.126	3.831	3.831	3.838	3.838	3.243	3.296	3.321	3.204	3.471
0.25	Exp.	1.94	2.09					3.25	3.275	3.35		
0.50	W	1.973	2.141	3.427	3.928	3.413	3.938	3.300	3.355	3.401	3.218	3.496
0.50	ZB	1.973	2.141	3.926	3.926	3.940	3.940	3.296	3.354	3.405	3.218	3.495
0.50	Exp.	1.96	2.12					3.30	3.355	3.40		
0.75	W	1.978	2.151	3.514	4.022	3.503	4.035	3.343	3.413	3.464	3.227	3.511
0.75	ZB	1.978	2.151	4.020	4.020	4.035	4.035	3.337	3.412	3.465	3.228	3.511
0.75	Exp.	1.96	2.12					3.35	3.395	3.46		
1.0	W		2.156			3.593	4.128			3.521	3.521	
1.0	ZB		2.156			4.128	4.128			3.521	3.521	
1.0	Exp.		2.15							3.53		

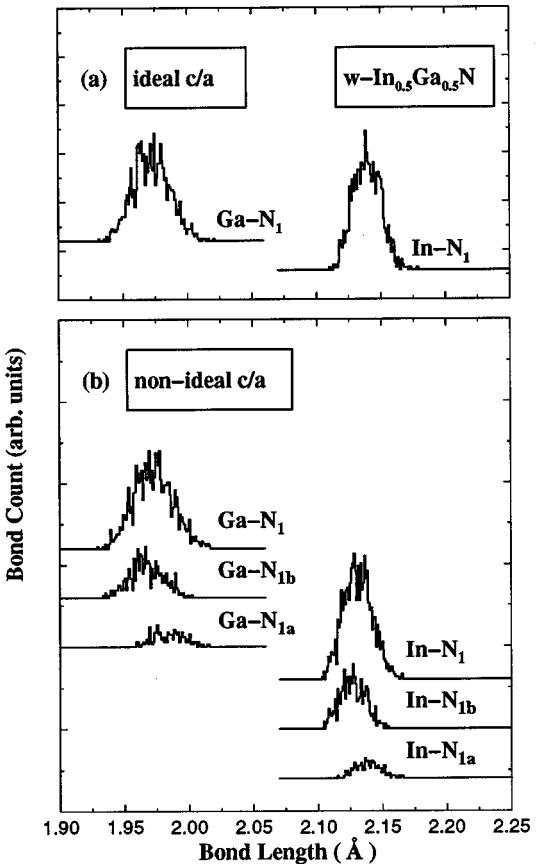

FIG. 2. The first-neighbor cation–anion bond length distributions in W $In_{0.5}Ga_{0.5}N$ alloy calculated assuming ideal and nonideal *c/a* ratio in the VFF method. The bonds $Ga–N_{1a,b}$ and $In–N_{1a,b}$ are illustrated in Fig. 1.

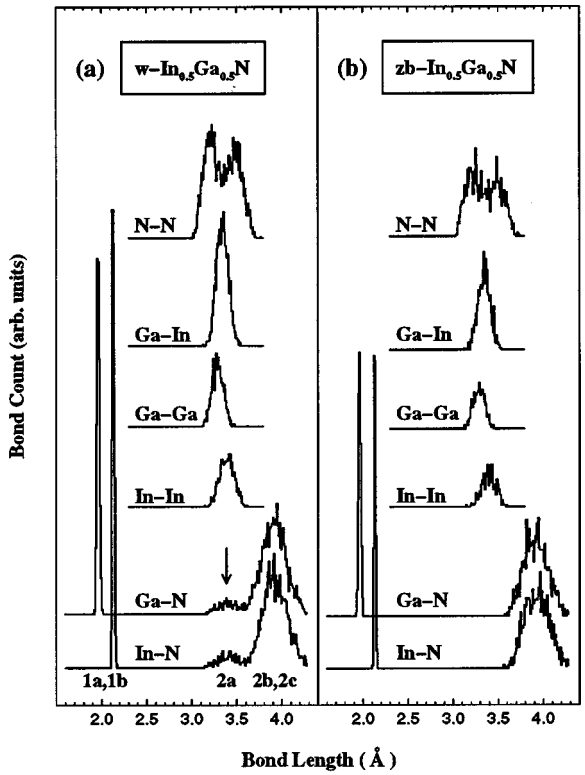

FIG. 3. The bond length distribution in (a) W and (b) ZB $In_{0.5}Ga_{0.5}N$ alloy. For the wurtzite structure ideal *c/a* ratio is assumed [method (A).]

(B) (Sec. II): for the Ga–N bond we see a small average expansion as expected based on the minor increase in the ideal Ga–N bonds when moving from ideal to nonideal *c/a* ratio. For In–N, the corresponding contraction is slightly larger due to the larger deviation of the *c/a* ratio from the ideal value in the InN binary.

C. First-neighbor cation–anion bonds: R_{A-C_1} vs R_{B-C_1}

Consistent with the results by Bellaiche *et al.*[9] we note in Fig. 2 that the first-neighbor cation-anion distance is split into a shorter $R^{w}_{\text{Ga-N}_1}$ bond and a longer $R^{w}_{\text{In-N}_1}$ bond. Figures 3(a) and 3(b) compare the bond distributions in W and ZB $In_{0.5}Ga_{0.5}N$ alloys. The first sharp peaks in Ga–N and In–N distribution correspond to $R_{\text{Ga-N}_1}$ and $R_{\text{In-N}_1}$. These two bonds have identical values in the W and ZB structures (the averaged peak positions are shown in Table IV). Since we are considering $In_{0.5}Ga_{0.5}N$, both first-neighbor peaks include the same amount of bonds (same integrated area). However, the $In–N_1$ peak is higher and narrower than the one for $Ga–N_1$, indicating a sharper distribution of the longer $In–N_1$ bonds than of the shorter $Ga–N_1$ bonds. This can be seen more clearly in Fig. 2 due to the higher resolution. We associate this with the smaller bond-bending force constant β (see Table I) for InN than for GaN: a small value for β means that less penalty is given for bond *angles* deviating from the ideal values and therefore the bond *length* can obtain a value closer to the ideal one (narrower distribution).

The second column of Table IV compares the first-neighbor cation–anion bond lengths at several compositions for W and ZB $In_xGa_{1-x}N$ alloy. Comparison between the calculated values reveals identical bonds in W and ZB structures at all compositions. Table IV also gives the experimental data points measured by the total electron yield extended x-ray absorption fine structure (TEY EXAFS) technique for samples grown using molecular beam epitaxy (MBE).[10] The samples appear not to exhibit either pure W or ZB structure, but contain amorphous parts in addition to the crystalline regions.[10] The calculated and experimental values are illustrated graphically in Fig. 4(a) as a function of the alloy composition for the W structure. The predicted bond lengths are shown by solid lines revealing a linear dependence on the alloy composition. The experimental values[10] are shown with cross markers. We find a good agreement between the calculated and experimental values.

D. Second-neighbor cation–anion bonds: $R^{w}_{A-C_2}$ vs $R^{zb}_{A-C_2}$

For second-neighbor cation–anion bonds we expect the significant difference between W and ZB forms as described in Eqs. (3) and (5). Indeed, Fig. 3(a) clearly shows that in the W structure we find two peaks corresponding to $R_{A-C_{2a}}$ (indicated by arrow) and $R_{A-C_{2b,c}}$, while in the ZB structure there is only one peak. The peak corresponding to $R_{A-C_{2a}}$ is much weaker than the dominant peak $R_{A-C_{2b,c}}$ due to 1:10

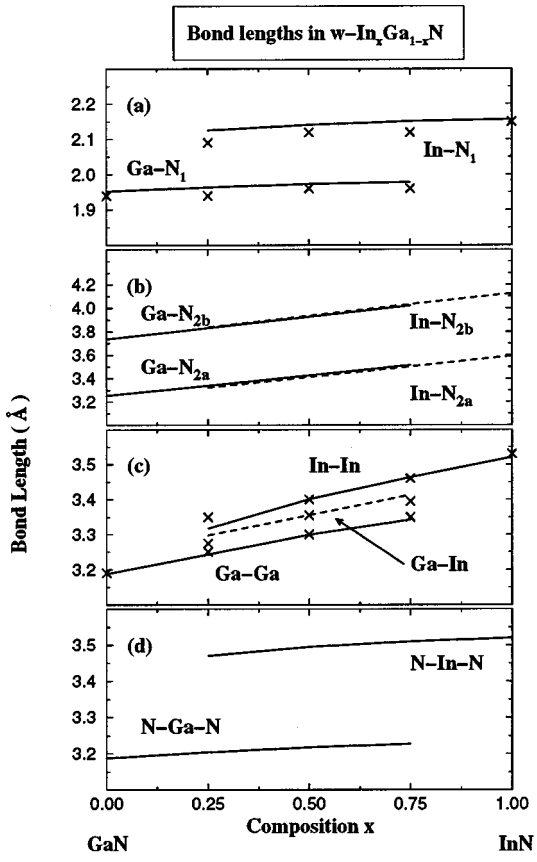

FIG. 4. Bond lengths in W $In_xGa_{1-x}N$, as a function of the alloy composition x. The calculated values are illustrated with lines, while the experimental data points (Ref. 10) are drawn with crosses where available. The types of bonds are explained in Fig. 1.

ratio between these types of bonds in the W structure [see Eq. (4)]. Therefore it might be overlooked in experiments with finite resolution or may be incorrectly assigned to an alloy-broadened part of the second-neighbor bonds. However, as Eq. (4) shows, the existence of a *split* second-neighbor cation-anion bond is an intrinsic property of the W structure, and already exists in pure compounds, irrespective of c/a and u.

E. Second-neighbor cation–anion bonds: R_{A-C_2} vs R_{B-C_2}

Figures 3(a) and 3(b) show that the $R_{\text{Ga-N}_2}$ and $R_{\text{In-N}_2}$ distances have nearly identical (cation independent) values in both W and ZB structures. This is in contrast with the first-neighbor distances $R_{\text{Ga-N}_1}$ and $R_{\text{In-N}_1}$ exhibiting distinct values. Rather, the effect of the alloy environment can be seen in the widths of the peaks which are much broader than for the peaks corresponding to first-neighbor cation–anion distances.

The distinction between first- and second-neighbor cation–bonds can be understood by considering the relative cation and anion displacements during alloy relaxation: to first order, cations (Ga and In) remain at their ideal fcc-lattice positions while anions (N) are displaced from their ideal sublattice sites in order to accommodate the nearest-neighbor bond lengths.[2] However, the *average* anion position stays ideal. Therefore, the $R_{\text{Ga-N}_2}$ and $R_{\text{In-N}_2}$ exhibit nearly an equal value which coincides with the value in unrelaxed alloy.

The third and fourth columns in Table IV show the second-neighbor cation–anion bond lengths for the investigated $In_xGa_{1-x}N$ alloy compositions. These values are graphically presented in Fig. 4(b) for the W structure. We again note the splitting between the $R^w_{A-C_{2a}}$ and $R^w_{A-C_{2b}}$ bonds, as well as the almost negligible cation dependence of the bond lengths. It is also evident that these second-neighbor cation–anion bonds have a stronger dependence on the alloy composition than the nearest-neighbor bonds $R_{\text{Ga-N}_1}$ and $R_{\text{In-N}_1}$. Currently, there are no experimental data available for the second-neighbor cation–anion bonds and the values in Table IV and Fig. 4(b) are offered as prediction.

F. Cation–cation and anion–anion bonds

The Ga–Ga, Ga–In, and In–In bonds shown in Fig. 3 exhibit three distinct values: the smallest distance is found for the Ga–Ga bond while In–In is the largest, and Ga–In between the two extremes. These three values are explained by the differing atomic radii of the cations. Both W and ZB structures exhibit nearly the same cation–cation bond lengths as shown in the fifth column in Table IV. The comparison between the calculated and experimental[10] values in Fig. 4(c) indicates good agreement. We also note that the dependence on the alloy composition for the cation–cation bonds is significantly larger than for the nearest-neighbor bonds in Fig. 4(a).

In the N–N bond distribution (Fig. 3) we see two distinct peaks. The origin of these peaks is the chemical identity of the intermediate cation: the shorter N–N bond corresponds to N–Ga–N configuration and the longer one to N–In–N configuration. The sixth column in Table IV reveals only

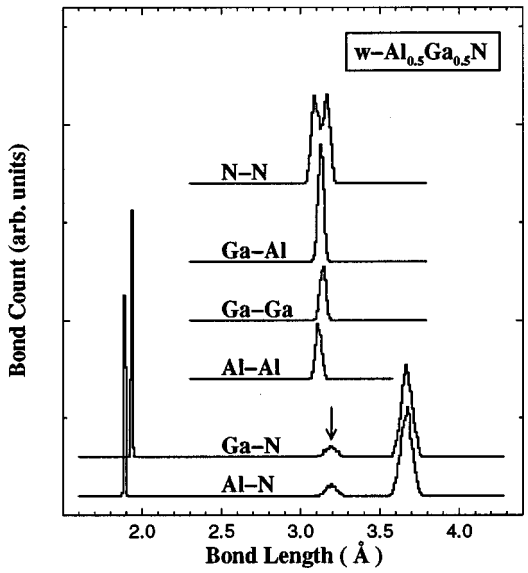

FIG. 5. The bond length distribution in W $Al_{0.5}Ga_{0.5}N$ alloy. Ideal c/a ratio is assumed in the calculations [method (A)].

TABLE V. Calculated values of the histogram average relaxed bond lengths (in angstroms) in $Al_xGa_{1-x}N$ alloy for various compositions. For W structure an ideal *c/a* ratio is assumed in the calculations.

x	Structure	$R_{Ga\text{-}N_1}$	$R_{Al\text{-}N_1}$	$R_{Ga\text{-}N_{2a}}$	$R_{Ga\text{-}N_{2b}}$	$R_{Al\text{-}N_{2a}}$	$R_{Al\text{-}N_{2b}}$	$R_{Ga\text{-}Ga}$	$R_{Ga\text{-}Al}$	$R_{Al\text{-}Al}$	$R_{N\text{-}N_a}$	$R_{N\text{-}N_b}$
0.0	w	1.949		3.248	3.732			3.183			3.183	
0.0	zb	1.949		3.732				3.183			3.183	
0.5	w	1.943	1.899	3.199	3.679	3.203	3.676	3.149	3.137	3.122	3.100	3.173
0.5	zb	1.943	1.899	3.679		3.676		3.150	3.137	3.121	3.100	3.173
1.0	w		1.892			3.153	3.623			3.090	3.090	
1.0	zb		1.892			3.623				3.090	3.090	

small differences between the anion–anion bond lengths between W and ZB alloys. The graphical illustration in Fig. 4(d) indicates again a linear dependence of the anion–anion bond lengths of the W alloy composition, with a slope similar to second-neighbor cation–anion bonds [Fig. 4(b)].

We note that qualitatively similar behavior of cation–cation and anion–anion bonds (slopes, splitting of the anion–anion bonds) has been observed in zinc-blende InGaAs alloys.[5,8,19]

IV. BOND LENGTHS IN $Al_xGa_{1-x}N$ ALLOY

The bond length distribution for W $Al_{0.5}Ga_{0.5}N$ alloy is shown in Fig. 5. In comparison with $In_{0.5}Ga_{0.5}N$ (Fig. 3) we note that the distribution peaks are much sharper, as expected based on the smaller lattice mismatch between AlN and GaN alloys. Also, the splitting between, e.g., $R_{Ga\text{-}N_1}$ and $R_{Al\text{-}N_1}$ is much smaller than in $In_{0.5}Ga_{0.5}N$. Otherwise, $Al_{0.5}Ga_{0.5}N$ alloy qualitatively reproduces all the essential features predicted for $In_{0.5}Ga_{0.5}N$ above. Table V shows the predicted bond lengths for $Al_xGa_{1-x}N$ alloy for $x=0,0.5,1$. We see that due to smaller lattice mismatch between AlN and GaN than InN and GaN the bond length dependence on the alloy composition is much smaller than in InGaN.

V. CONCLUSION

We have investigated the bond lengths in W and ZB InGaN and AlGaN alloys using the VFF simulations and large (512–1280 atom) supercells.

Our results show that while the first-neighbor cation–anion bonds for *different cations* (R_{A-C_1} and R_{B-C_1}) retain distinct values in the studied W and ZB alloys, the second-neighbor cation–anion bonds R_{A-C_2} and R_{B-C_2} merge into a single bond length. However, the second-neighbor cation–anion bonds for the *same cation* exhibit a crucial difference between W and ZB structures: in W we find *two* bond distances which differ in length by about 13% while in the ZB structure there is only *one* bond length. This is an intrinsic property of the binary constituents and persists in the alloys. Also, the small splitting of the first-neighbor cation–anion bonds in the W structure is preserved in the alloy, but obscured by the bond length broadening. The calculated cation–cation and anion–anion bond lengths are shown to exhibit almost identical values in the W and ZB structures. The cation–cation bonds exhibit three distinct values corresponding to *A–A*, *A–B*, and *B–B* bonds. The anion–anion bonds are split into two principal cation-dependent values (*C–A–C* and *C–A–C*). For all the studied bond lengths we predict a nearly linear dependence on alloy composition. The bond length broadening and dependence on the alloy concentration is found to be much larger in InGaN alloy than in AlGaN alloy due to larger lattice mismatch between the constituents.

For InGaN the predicted results are in good agreement with the experimental data[10] available for R_{A-C_1}, R_{B-C_1}, R_{A-A}, R_{B-B}, and R_{A-B} bonds. However, the most important predictions still awaiting experimental testing are: (i) $R^w_{A-C_{2a}}$ and $R^w_{A-C_{2b,c}}$ are predicted to be clearly split in the W alloys; (ii) the first-neighbor anion–anion distance is predicted to be split into two values originating from the *C–A–C* and *C–B–C* configurations; (iii) although qualitatively similar to InGaN, the broadening of the bond lengths and cation-related splitting of the bonds have a much smaller magnitude in AlGaN alloy due to smaller lattice mismatch.

ACKNOWLEDGMENTS

The authors thank the authors of Ref. 10 for providing us with their experimental values prior to publication. We thank S.-H. Wei for helpful discussions. T.M. acknowledges the financial support by the Väisälä Foundation (Helsinki, Finland). This work is supported in part by the U.S. Department of Energy, OER-BES-DMS, Grant No. DE-AC36-83-CH10093.

[1] J. C. Wooley, in *Compound Semiconductors*, edited by R. K. Williardson and H. L. Goering (Reinhold, New York, 1962), p. 3; C. Fong and J. C. Phillips, Phys. Rev. B **14**, 5387 (1976).
[2] C. Mikkelsen and J. B. Boyce, Phys. Rev. Lett. **49**, 1412 (1982); Phys. Rev. B **28**, 7130 (1983); J. B. Boyce and J. C. Mikkelsen, *ibid.*, **31**, 6903 (1985).
[3] A. Balzarotti, M. T. Czyzyk, A. Kiesiel, N. Motta, M. Podgorny, and M. Zimnal-Starnawska, Phys. Rev. B **30**, 2295 (1984).
[4] A. Balzarotti, N. Motta, A. Kiessiel, M. Zimnal-Starnawska, M. T. Czyzyk, and M. Podgorny, Phys. Rev. B **31**, 7526 (1985).
[5] N. Motta, A. Balzarotti, P. Letardi, A. Kiesiel, M. T. Czyzyk, M. Zimnal-Starnawska, and M. Podgorny, Solid State Commun. **53**, 509 (1985).
[6] J. L. Martins and A. Zunger, Phys. Rev. B **30**, 6217 (1984).
[7] C. K. Shih, W. E. Spicer, W. A. Harrison, and A. Sher, Phys. Rev. B **31**, 1139 (1985).
[8] Y. Cai and M. F. Thorpe, Phys. Rev. B **46**, 15879 (1992).
[9] L. Bellaiche, S.-H. Wei, and A. Zunger, Phys. Rev. B **56**, 13872 (1997).
[10] N. J. Jeffs, A. V. Blant, T. S. Cheng, C. T. Foxon, C. Bailey, P. G. Harrison, A. J. Dent, and J. F. W. Mosselmans, Proceedings of MRS March Meeting, San Francisco, 1998.

[11] H. Morkoç, S. Strite, G. B. Gao, M. E. Lin, B. Sverdlov, and M. Burns, J. Appl. Phys. **76**, 1363 (1994).
[12] S. Strite and H. Morkoç, J. Vac. Sci. Technol. B **10**, 1237 (1992).
[13] C.-Y. Yeh, Z. W. Lu, S. Froyen, and A. Zunger, Phys. Rev. B **46**, 10086 (1992).
[14] A. Zunger, in *Handbook of Crystal Growth*, edited by D. T. J. Hurle (Elsevier, Amsterdam, 1994), Vol. 3, p. 999.
[15] P. N. Keating, Phys. Rev. **145**, 637 (1966).
[16] R. M. Martin, Phys. Rev. B **1**, 4005 (1970).
[17] K. Kim, W. R. L. Lambrecht, and B. Segall, Phys. Rev. B **53**, 16310 (1996).
[18] W. H. Press, B. P. Flannery, S. A. Teukolsky, and W. T. Vetterling, *Numerical Recipes* (Cambridge, New York, 1986), pp. 305–306.
[19] A. Silverman, A. Zunger, R. Kalish, and J. Adler, Phys. Rev. B **51**, 10795 (1995).